ORNL/TM--9486

DE85 007305

Engineering Physics and Mathematics Division

MONTE CARLO STUDIES OF URANIUM CALORIMETRY*

J. Brau and H. J. Hargis
University of Tennessee

T. A. Gabriel and B. L. Bishop+
Oak Ridge National Laboratory

*Submitted for Journal publication

+Computing & Telecommunications

NOTICE This document contains information of a preliminary nature. It is subject to revision or correction and therefore does not represent a final report.

Date of Issue: January 1985

Research sponsored by
U.S. Dept. of Energy
Office of High Energy
and Nuclear Physics

Prepared by the
Oak Ridge National Laboratory
Oak Ridge, Tennessee 37831
operated by Martin Marietta Energy Systems, Inc.
for the U.S. DEPARTMENT OF ENERGY
under Contract No. DE-AC05-840R21400

TABLE OF CONTENTS

ABSTRACT

Detailed Monte Carlo calculations of uranium calorimetry are presented which reveal a significant difference in the responses of liquid argon and plastic scintillator in uranium calorimeters. Due to saturation effects, neutrons from the uranium are found to contribute only weakly to the liquid argon signal. Electromagnetic sampling inefficiencies are significant and contribute substantially to compensation in both systems.

INTRODUCTION

The use of uranium as the inactive medium in sampling calorimeters has resulted in the best resolution for hadronic shower measurements thus far achieved.[1,2] The neutrons produced by nuclear fission in the uranium have been found to compensate for the inherent shower fluctuations, leading to resolutions of $\sim$ 30-35%/$\sqrt{E}$ for calorimeters using either liquid argon or plastic scintillator as the active medium.

We report here new detailed Monte Carlo calculations of these calorimeters that suggest that the sampling inefficiencies for electromagnetic showers in uranium calorimeters contributed significantly to the observed compensation. Furthermore, saturation in liquid argon is an important effect; due to this, liquid argon as a sampling medium does not fully respond to the neutrons and does not achieve as good a resolution with uranium as plastic scintillator does. That these electromagnetic sampling inefficiency effects, sometimes referred to as "transition effects," should be important has previously been noted.[3,4] Here we quantify their contribution and also investigate the resulting compensation in a lead-liquid argon calorimeter.

METHOD OF CALCULATION

The calculations were performed with the CALOR computer system following approximately the procedures used in previous calculations.[5,6] A flow diagram of the codes in CALOR is given in Fig. 1. The three-dimensional, multimedia, high-energy nucleon-meson transport code (HETC)[7] was used, with modifications, to obtain a detailed description of the nucleon-meson cascade produced in the devices considered in this paper. This Monte Carlo code takes into account the slowing down of charged particles via the continuous slowing-down approximation, the decay of charged pions and muons, inelastic nucleon-nucleus and charged-pion-nucleus (excluding hydrogen) collisions through the use of the intermediate-energy intranuclear-cascade-evaporation (MECC) model ($E < 3$ GeV) and scaling model ($E > 3$ GeV), and inelastic nucleon-hydrogen and charged-pion-hydrogen collisions via the isobar model ($E < 3$ GeV) and phenomenological fits to experimental data ($E > 3$ GeV). Also accounted for are elastic neutron-nucleus collisions ($E < 100$ MeV), and elastic nucleon and charged-pion collisions with hydrogen.

The intranuclear-cascade-evaporation model as implemented by Bertini is the heart of the HETC code.[8] This model has been used for a variety of calculations and has been shown to agree quite well with many experimental results. Even when agreement is not very good, the results produced by this model can lead the user to make correct decisions. The underlying assumption of this model is that particle-nuclear interactions can be treated as a series of two-body collisions within the nucleus and that the location of the collision and resulting particles from the collision are governed by experimental and/or theoretical particle-particle total and differential cross-section data. The types of particle collisions included in the calculations are elastic, inelastic and charge exchange. This model incorporates the diffuseness of the nuclear edge, the Fermi motion of the bound nucleons, the exclusion principle, and a local potential for nucleons and pions. The density of the neutrons and protons within the nucleus (which is used with the total cross section to determine interaction locations) are determined from the experimental data of Hofstadter.[8] Nuclear potentials are determined from these density profiles by using a zero-temperature Fermi distribution. The total well depth is then defined as the Fermi energy plus 7 MeV. Following the cascade part of the interaction, there is

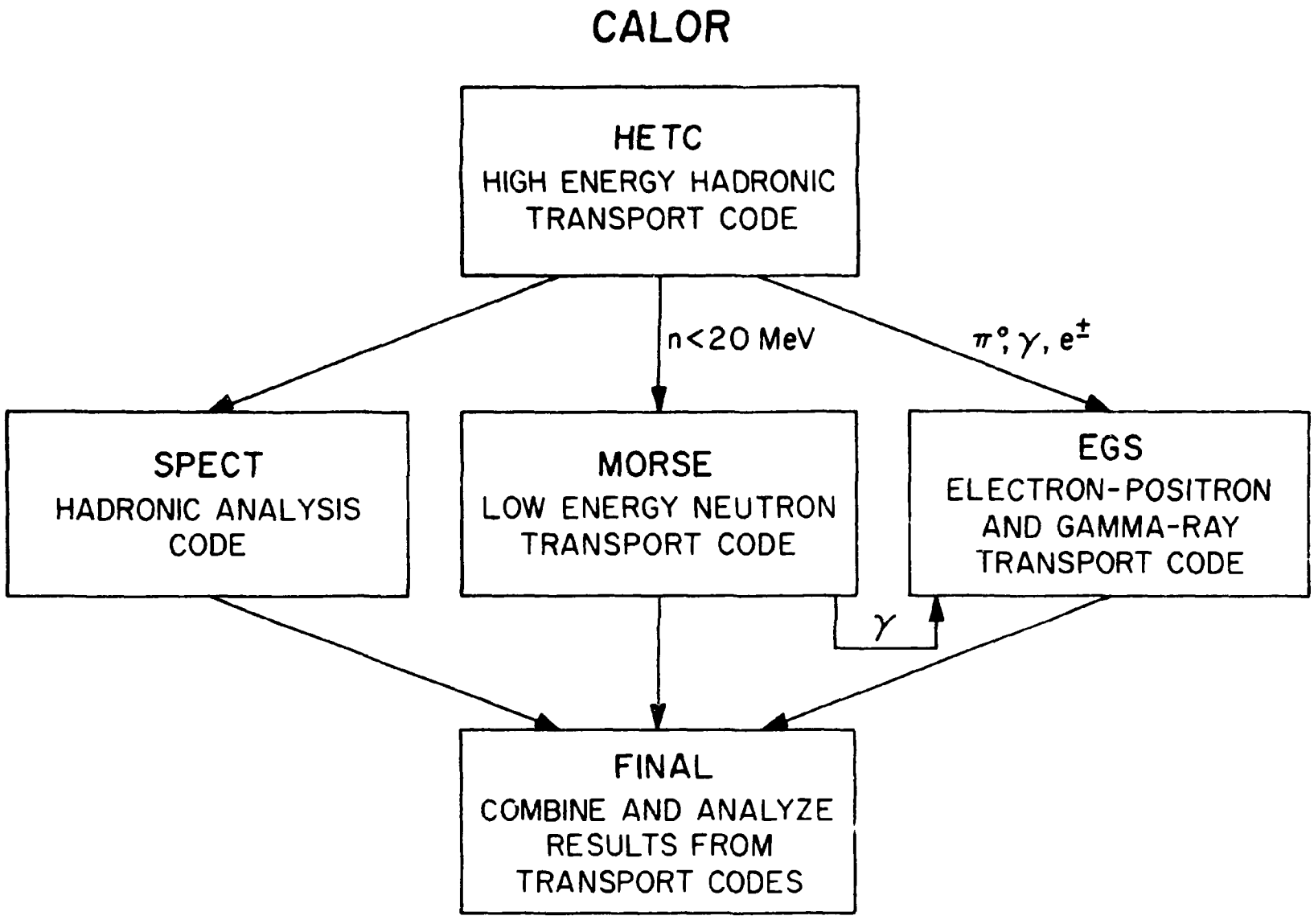

Fig. 1. Flow diagram of the CALOR computer system.

excitation energy left in the nucleus. This energy is treated by using an evaporation model which allows for the emission of protons, neutrons, d, ^{3}He, α, and T. Fission induced by high-energy particles is accounted for during this phase of the calculation by allowing it to compete with evaporation. Whether or not a detailed fission model is included has very little effect on the total number of secondary neutrons produced.

The source distribution for the electromagnetic cascade calculation is provided by HETC; it consists of photons from neutral pion decay, electrons and positrons from muon decay (although this is usually not of interest in calorimeter calculations because of the long muon lifetime), deexcitation gamma rays from inelastic nuclear collisions, and fission gamma rays. Since the discrete decay energies of the deexcitation gammas are not provided by HETC and only the total energy is known, individual gamma energies are obtained by uniformly sampling from the available energy until is completely depleted. The transport of the electrons, positrons, and gammas from the above sources is carried out using the EGS system.[9]

Neutrons which are produced with energies below 20 MeV are transported using the MORSE[10,11] Monte Carlo transport code. The neutron cross sections used by MORSE were obtained from ENDFB/IV. Gamma rays (including those from capture, fission, etc.) produced during this phase of the calculations are stored for transport by the EGS code. The MORSE code was developed for reactor application and can treat fissioning systems in detail. This ability is very important since a majority of the fission compensation results from neutrons with energies less than 20 MeV. Time dependence is included in MORSE, but since neither HETC nor EGS has a timing scheme incorporated, it has been assumed that no time passes for this phase of the particle cascade. Therefore, all neutrons below 20 MeV are produced at t = 0. General time cuts used in the MORSE code are 50 nsec for scintillator and 100 nsec for liquid argon.

The nonlinearity of the light pulse or charge collected (L) due to saturation effects is taken into account by the use of Birk's Law,[12]

$$\frac{dL}{dx} \propto \frac{dE/dx}{1+kB\ dE/dx} ,$$

where kB is the saturation constant. For the scintillators studied, kB = 0.01 gm/cm^2/MeV or 0.02 gm/cm^2/MeV, while for the liquid argon, we have assumed kB = 0.0045 gm/cm^2/MeV. The liquid argon value is based on the assumption that a 5-MeV alpha particle gives the same signal as a 1.25-MeV electron.[1] This takes into account the loss of signal resulting from recombination effects in the ionization column.[13] For electrons at all energies, it is assumed that kB = 0.

URANIUM–LIQUID ARGON HEXAGONAL CALORIMETER

The hexagonal calorimeter of reference 1 consists of 5.1 interaction lengths of central modules of uranium–liquid argon (1.7-mm uranium plates and 2-mm argon gaps) surrounded and backed up by iron-liquid argon modules. This geometry has been approximated in these calculations with cylindrical geometry as in reference 6. Figure 2a shows the calculated

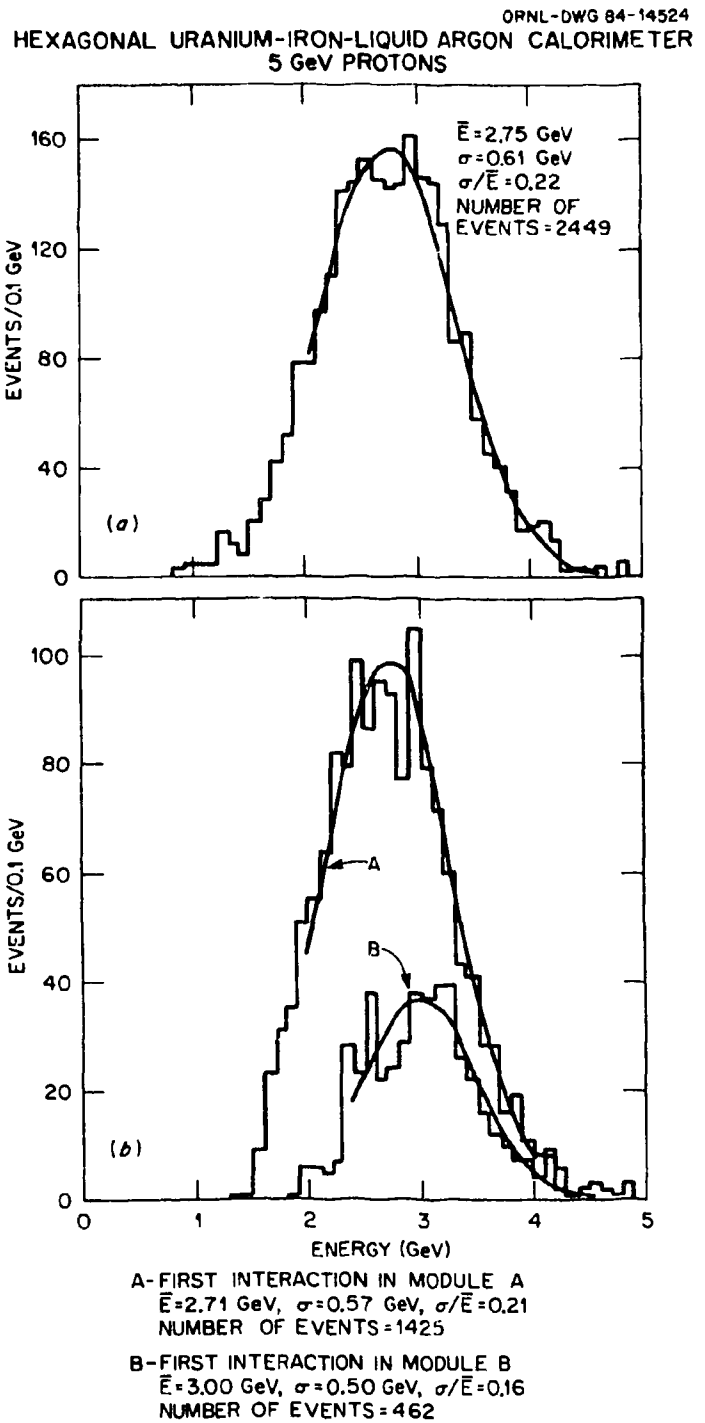

Fig. 2. (a) Calculated energy distribution for 5-GeV protons incident on the hexagonal uranium-liquid argon calorimeter of reference 1. (b) Calculated energy distribution for 5-GeV protons incident on the hexagonal uranium-liquid argon calorimeter of reference 1 when the first interaction occurs in module A or module B.

energy distribution for 5-GeV protons incident upon this hexagonal uranium calorimeter. These calculations were repeated for incident $\pi^{\pm}$'s with similar results. The energy detected in each module was individually weighted to account for the fraction of the energy loss appearing in the liquid argon by multiplying the energy in the liquid argon gap by

$$\frac{dE/dx|Ar_{min}\ X_{Ar} + dE/dx|i_{min}\ X_i}{dE/dx|Ar_{min}\ X_{Ar}}, \qquad (1)$$

where $dE/dx|i_{min}$ is the minimum energy loss for medium i taken from the Particle Data Group tables[14] and X_i's are the respective thicknesses of the active and inactive regions. The weight factors for the iron sections were increased by 20% as in reference 1. This distribution shows a resolution of $\sigma/E = 0.22$ when fit to a Gaussian distribution starting at the half-peak point on the low-energy side. This corresponds to a resolution of $\sigma/E = 0.50/\sqrt{E}$.

We can compare this calculation to the test data reported in reference 1. These results have demonstrated hadronic resolutions of about $30\text{-}35\%/\sqrt{E}$ in a uranium–liquid argon calorimeter, but not for a full calorimeter. The results presented in reference 1 are based on showers for which the first interaction occurs in module B. Module B begins after the 1.7 interaction lengths of module A, meaning that a small fraction (less than or equal to 20%) of the showers pass this selection. Figure 2b shows the calculated energy distribution for the showers of Fig. 2a which have their first interaction in region B. Showers were identified as having their first interaction in region A when the pulse height seen in region A was greater than four times the pulse height of a minimum ionizing particle. Those not so selected were identified with region B when the pulse height seen in region B was more than four times minimum ionization. We see that the resolution for the showers selected for region B is improved ($\sigma/E = 0.16$), as is the case for the experimental data. However, this resolution for restricted showers should not be interpreted as the overall resolution of the calorimeter since it represents less than 20% of the incident particles.

The results of reference 1 also include an iron–liquid argon calorimeter of similar geometry to the uranium–liquid argon case. Figure 3 shows the calculated energy distribution for 5-GeV protons incident upon this iron–liquid argon geometry. The Gaussian fit gives a resolution of 20%, in good agreement with the value reported in Fig. 11 of reference 1. Note that this is comparable to the uranium–liquid argon case when all showers are retained, although the sampling fluctuations make a larger contribution to the uranium–liquid argon case.

The e/h (electron/hadron) ratios were calculated for both the uranium and the all-iron hexagonal calorimeters of reference 2. The values calculated (as shown in Table 1) are 1.1 and 1.5 compared with the reported measurements of 1.1 and 1.5, in perfect agreement. However, the principal mechanism responsible for reducing e/h in uranium–liquid argon is the electromagnetic sampling inefficiency, not fission. Just as fission has been envisioned to equalize the response of a calorimeter to the electromagnetic and nuclear components of a hadron-initiated cascade, the electromagnetic sampling inefficiency occurs when the active and inactive media have much different responses to the electromagnetic cascade (e.g., critical energies, low-energy photon attenuation, multiple scattering, etc.). The fission process works through amplification of the nuclear component, while the electromagnetic sampling inefficiency, in a parallel way, works through suppression of the electromagnetic component.

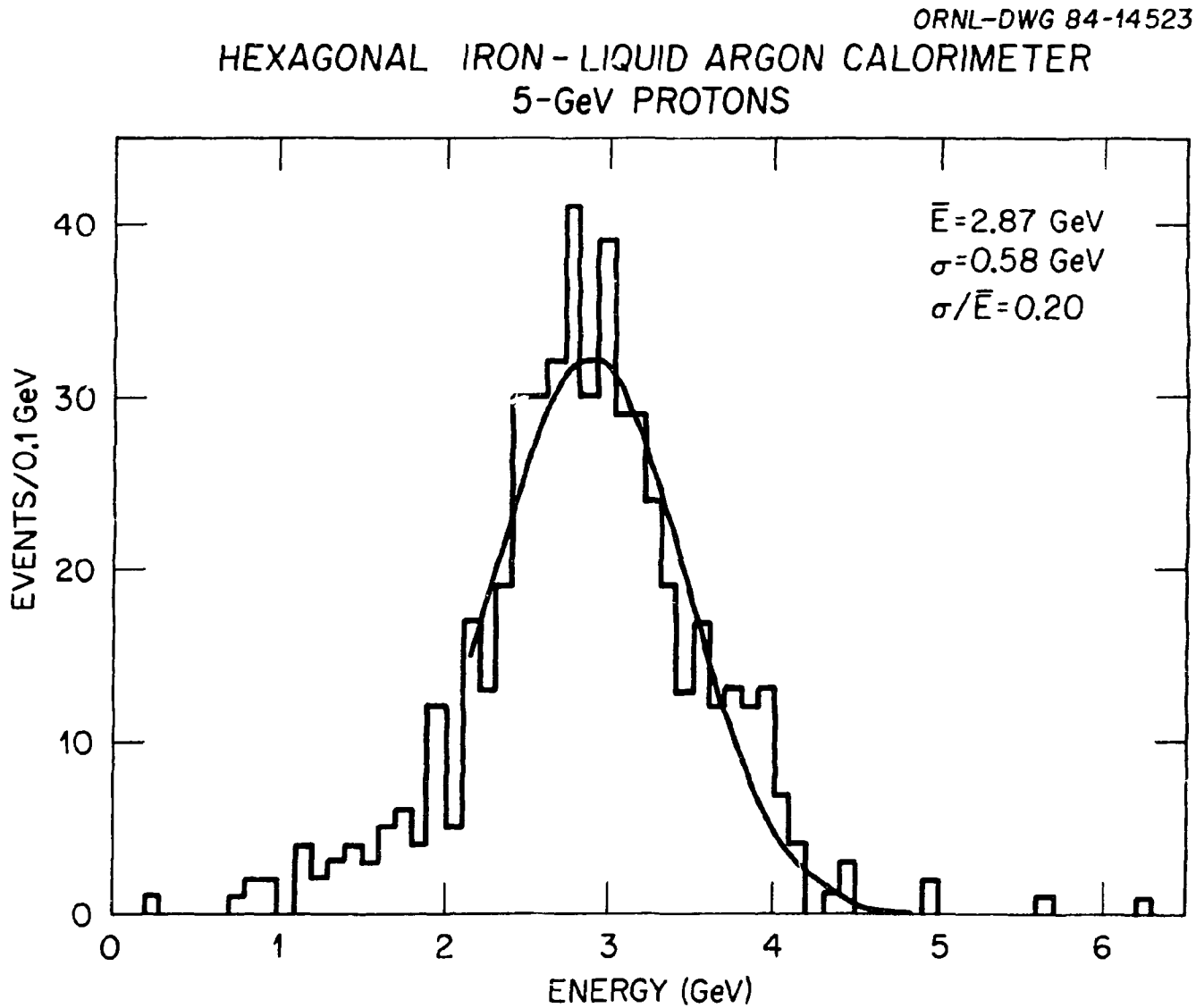

Fig. 3. Calculated energy distribution for 5-GeV protons incident on an all-iron hexagonal uranium–liquid argon calorimeter of reference 1.

Table 1

Summary of Calculated e/h Ratios Compared to Data

	e/h	
	Data	Monte Carlo
Iron-Liquid Argon Hexagonal Calorimeter		
All Interactions		1.7
Restricted First Interactions in B	1.5	1.5
Uranium-Liquid Argon Hexagonal Calorimeter		
All Interactions		1.2
Restricted First Interactions in B	1.1	1.1
AFS All-Uranium	1.1	0.9(1.02)*
AFS 50-50 Copper-(Iron)-Uranium	1.2	1.0(1.12)
AFS All Copper-(Iron) Catcher	1.4	1.4(1.53)

*kB = 0.01 gm/cm^2/MeV (kB = 0.02 gm/cm^2/MeV).

The conclusions drawn here differ from those in an earlier paper on uranium liquid-argon calorimetry[6] due to two changes which make the present analysis more reliable. First, the transport of photons and electrons is now followed by EGS. The earlier calculations used a modified version of the code developed by Beck[5] in which multiple scattering was neglected and all processes, except Compton scattering, were assumed to emit products in the same direction as the particle producing the interaction. Secondly, saturation effects have been accounted for by Birk's Law, as described earlier.

THE AFS URANIUM CALORIMETER

Another uranium calorimeter (the AFS and the ISR) has obtained $\sim 35\%/\sqrt{E}$ resolution with plastic scintillator. As shall be shown, the scintillator is more effective than liquid argon in transferring the neutron energy to output signal.

The AFS calorimeter consists of thin uranium plates (2 and 3 mm) separated by scintillator. The AFS collaboration has also reported results of tests with varying mixtures of copper and uranium plates[2] and also results of a test on a copper catcher[15] (an all-copper-scintillator calorimeter). Data on copper were unavailable for the calculations, but since iron and copper have similar properties, iron data were substituted for the copper data.

Two uranium cases were calculated to simulate the AFS calorimeters of reference 2: an all-uranium calorimeter and a calorimeter consisting of a 50-50 mix of iron and uranium. A third all-iron case was done to simulate the copper catcher of reference 15.

The all-uranium and uranium-iron calorimeters were each 60 cm x 120 cm in cross section and of lengths specified in reference 2. The all-uranium calorimeter contained 395 mm of uranium and 337.5 mm of scintillator (3.81 absorption lengths), and the uranium-iron calorimeter contained 161 mm of uranium, 265 mm of iron, and 290 mm of scintillator. The "iron catcher" was 64.2 cm by 50 cm in cross section (somewhat smaller than the uranium calorimeters) and had a depth of 75 cm.

The calculations were performed for 5-GeV π^-'s incident on all three calorimeters. As noted earlier, two different values were assumed for the saturation constant kB — 0.01 and 0.02 gm/cm^2/MeV. The results are shown in Figs. 4a-c and 5a-c, respectively, with superimposed Gaussian curves fitted in the same way as the data were fit by the authors of references 2 and 15. The observed signals in the scintillators were scaled in a similar fashion to Eq. (1) of the previous section.

Table 2 compares the resolutions determined from the Monte Carlo energy distributions with those of the published data.[2,15] The agreement is remarkably good, with the all-uranium-scintillator calorimeter showing $\sim$35-40%/$\sqrt{E}$. One might wonder to what extent the restricted area of the all-iron-scintillator calorimeter is responsible for its worse resolution. Calculations carried out for this calorimeter with a surface area of 60 cm x 120 cm (the same as that of the AFS uranium calorimeters) yielded a resolution of 22%, which is still much worse than the resolutions for the uranium cases.

For comparison to the uranium–liquid argon case, it is interesting to consider the resolution for showers occurring in a restricted region of the calorimeter. When the first interaction for a 5-GeV π^- in the all-uranium calorimeter was required to occur at a depth of 25 to 50 cm, the calculated resolution became 13%, somewhat better than the overall resolution.

Why is the AFS calorimeter so much better than the uranium-liquid argon calorimeter? The answer lies in the transfer of the fission energy and low-energy neutrons from spallation reactions from the uranium through the sampling medium to an electrical signal and the role of saturation in this process. Table 3 shows the fraction of the measured energy appearing in each of the four categories tallied. The low-energy neutrons transfer much less energy to detectable signal in the liquid argon than in the scintillator. The mechanism behind this is saturation. For a given density of ionization in the two media, the scintillator has much larger saturation, but the hydrogen which is scattered in the scintillator by the neutrons gives lower dE/dx losses (less dense ionization) than those resulting from scattered argon ions in the liquid argon. Possibly coupling a hydrogenous medium to the liquid argon might result in better neutron coupling.

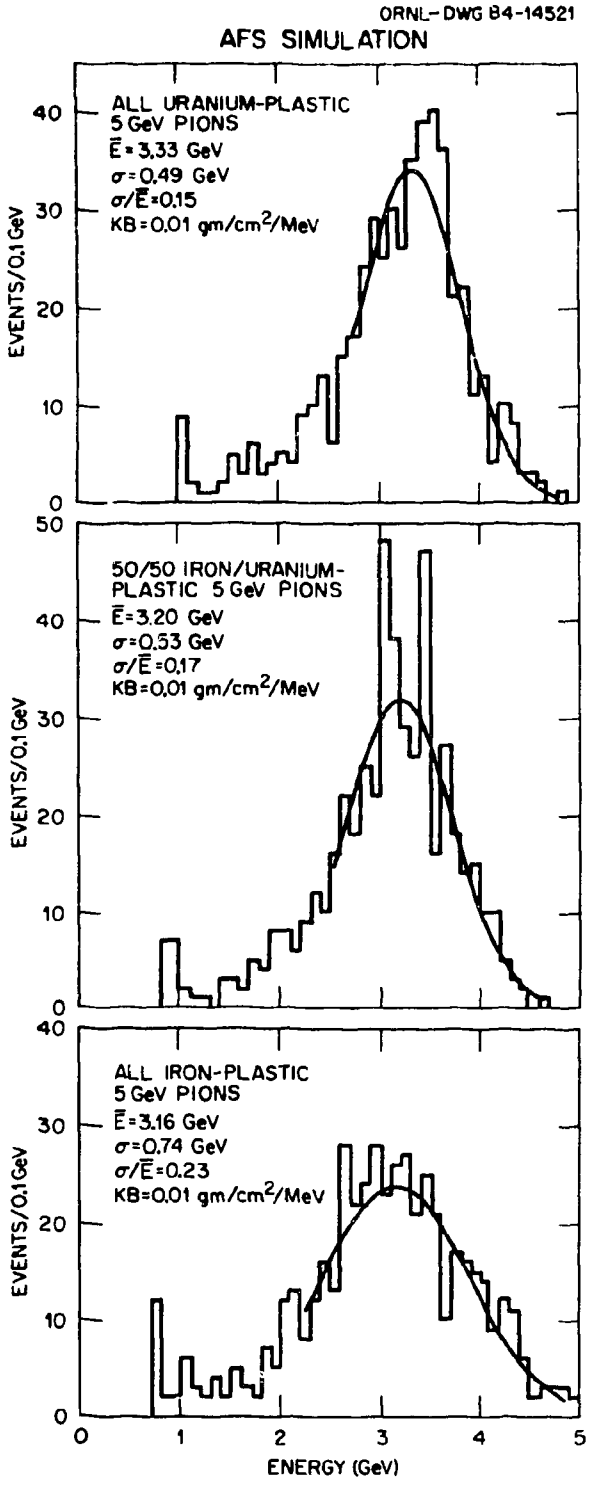

Fig. 4. Calculated energy distribution for 5-GeV π^-'s incident on the AFS-like uranium-iron scintillation calorimeters simulating references 2 and 15 with kB = 0.01 gm/cm^2/MeV.

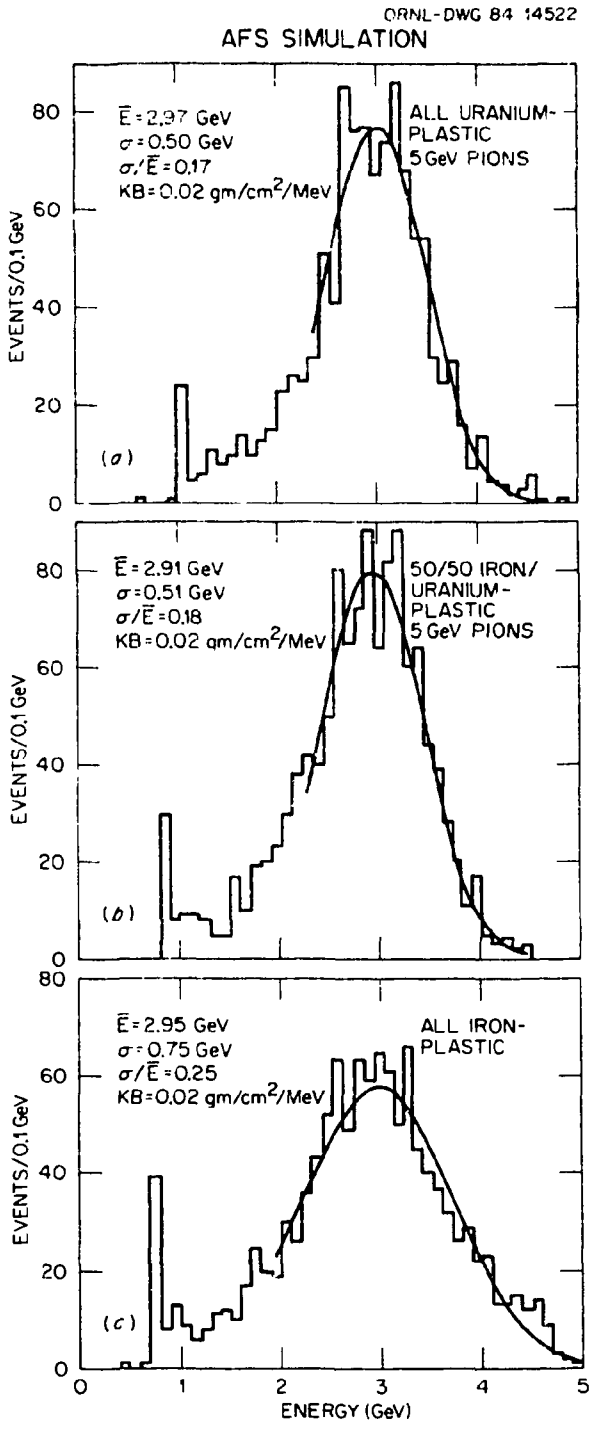

Fig. 5. Calculated energy distribution for 5-GeV π^-'s incident on the AFS-like uranium-iron scintillation calorimeters simulating references 2 and 15 with kB = 0.02 gm/cm^2/MeV.

Table 2

Comparison of Resolutions of Published Data With Those of Monte Carlo Calculations

Calorimeter	$\sigma/\sqrt{E}$ (5 GeV)	
	Data*	Monte Carlo**
AFS All-Uranium	33 ± 1	33(37)†
AFS 50-50 Copper-(Iron)-Uranium	38 ± 1	37(39)
AFS All-Copper-(Iron) Catcher	51	52(56,52)

*Fit to data in range of 2 to 10 GeV.
**Determined at 5 GeV.
†kB = 0.01 gm/cm^2/MeV (kB = 0.02 gm/cm^2/MeV).

The e/h ratios for the AFS calorimeter have been examined to see how they compare with the data. Values of 0.9 have been calculated at 2 and 5 GeV for kB = 0.01 gm/cm^2/MeV, while the reported experimental ratios are 1.1. The Monte Carlo calculations show slightly lower e/h values, or more compensation, than the data. This is probably due to several factors. The kB of the scintillating plastic used in the experiment is larger. When the KB value is increased to 0.02 gm/cm^2/MeV, the e/h ratio agrees better, while the resolutions are reasonably consistent as well (Tables 1 and 2).

LEAD–LIQUID ARGON CALORIMETERS

Since we have interpreted the compensation effects seen in the uranium-liquid argon calorimeter as being due largely to electromagnetic sampling inefficiencies, one would expect this improvement to be seen in calorimeters which employ other high-Z inactive regions. We have calculated the expected response for a calorimeter based on 2-mm-thick lead plates with 2-mm liquid argon gaps. Figure 6 shows the energy distribution for this calorimeter of depth 1.44 m with energy collected only over a radius of 20 cm. The observed resolution is 22% at 5 GeV. That this resolution is comparable to the resolution computed for the uranium–liquid argon calorimeter follows directly from the supposition that the sampling medium is unable to fully detect the fission amplification seen in scintillators and that the electromagnetic sampling inefficiencies found in high-Z sampling calorimeters are important. The ratio of electromagnetic-to-hadronic response is calculated to be 1.35. The excellent response to the lead–liquid scintillator calorimeter reported by Duffy et al.[16] is further support to this supposition.

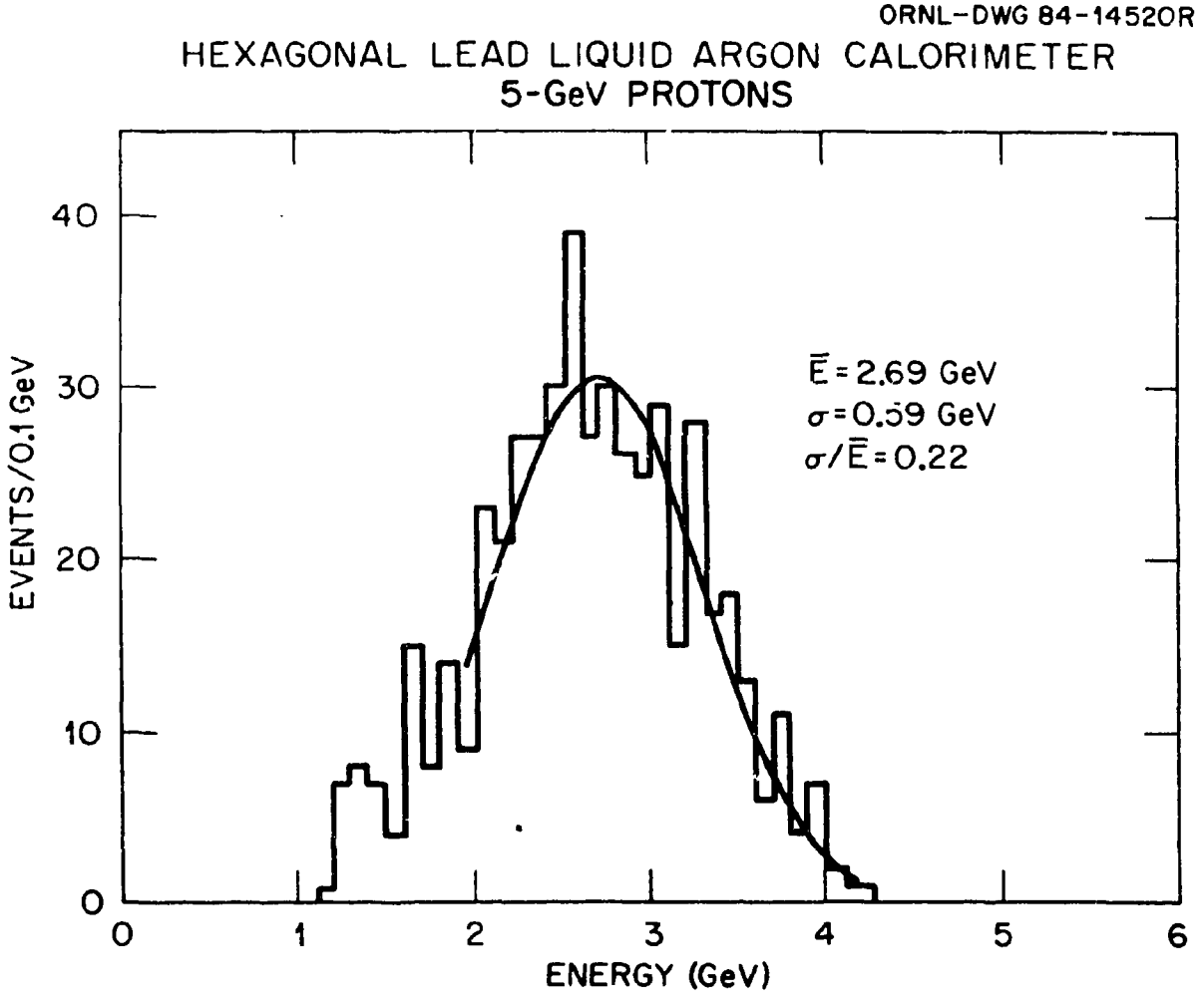

Fig. 6. Energy distribution for 5-GeV π^-'s incident on a 1.44-m-deep calorimeter of 2-mm lead plates separated by 2-mm liquid argon gaps. The energy is collected over a radius of 20 cm.

Table 3
Calculated Fractional Energy Distribution for 5-GeV Hadrons in the Hexagonal Uranium–Liquid Argon Calorimeter of Reference 1 and the AFS All-Uranium Scintillator Calorimeter of Reference 2.

	Fractional Energy	
	Hexagonal U-LA	AFS
Primary and secondary pions, protons, muons, and nuclear-recoil and evaporated-charged particles produced by protons and pions and neutrons with E > 20 MeV	0.65	0.49
Neutrons with E < 20 MeV	0.02	0.27
Deexcitation gamma rays	0.11	0.06
Electromagnetic from π^0 decay	0.22	0.18

CONCLUSIONS

The Monte Carlo calculations described in this paper indicate that pure liquid argon as a sampling medium does not produce the fine resolution which can be achieved by uranium-scintillator calorimeters such as the AFS at the ISR.[17] That liquid argon may have appeared experimentally to do so was at least partially due to event selection. The liquid argon is much less effective in coupling to the energy of the low-energy neutrons, resulting in some deficiency in the compensation mechanism. Furthermore, the compensation mechanism of electromagnetic sampling inefficiencies is important and plays a dominant role in compensation in liquid argon calorimeters.

REFERENCES

1. C. W. Fabjan et al., *Nucl. Instrum. Methods* **141**, 61 (1977).
2. O. Botner et al., *IEEE Transactions on Nuclear Science* **NS-28**, 510 (1981).
3. U. Amaldi, *Physica Scripta* **23**, 409 (1981).
4. O. Botner et al., *Physica Scripta* **23**, 556 (1981).
5. T. A. Gabriel and W. Schmidt, *Nucl. Instrum. Methods* **134**, 271 (1976).
6. T. A. Gabriel, *Nucl. Instrum. Methods* **150**, 146 (1978).
7. K. C. Chandler and T. W. Armstrong, "Operating Instructions for the High-Energy Transport Code HETC," ORNL-4744, Oak Ridge National Laboratory (1972).
8. H. W. Bertini, *Phys. Rev.* **188**, 1711 (1969).
9. R. L. Ford and W. R. Nelson, "The EGS Code System Computer Programs for the Monte Carlo Simulation of Electromagnetic Cascade Showers (Version 3)," SLAC-0210 (1978).
10. M. B. Emmett, "The MORSE Monte Carlo Radiation Transport Code System," ORNL-4972, Oak Ridge National Laboratory (1975).
11. N. M. Greene et al., "AMPX: A Modular Code System for Generating Coupled Multigroup Neutron-Gamma Libraries from ENDF/B," ORNL/TM-3706, Oak Ridge National Laboratory (1973).
12. J. B. Birks, *Proc. Phys. Soc.*, **A64**, 874 (1951).
13. W. Hofman et al., *Nucl. Instrum. Methods* **151** (1976).
14. Particle Data Group, *Reviews of Modern Physics* **56**, S1 (1984).
15. O. Botner et al., *Nucl. Instrum. Methods* **179**, 45 (1981).
16. M. E. Duffy et al., "Characteristics of a Lead Scintillator Calorimeter Used to Detect Electron Neutrinos," WISC-EX-84-239, University of Wisconsin, Madison, WI (1984).
17. J. E. Brau and T. A. Gabriel, "A Monte Carlo Study of Hadronic Calorimetry with Uranium," SLD-New Detector Note No. 119 (May 22, 1984).

ACKNOWLEDGEMENTS

These results have benefited from our discussions with W. Bugg, D. Hitlin, A. Lankford, P. Mockett, P. Rehak, R. Schindler, M. Shaevitz, and W. Willis.

INTERNAL DISTRIBUTION

1. L. S. Abbott
2. F. S. Alsmiller
3. R. G. Alsmiller, Jr.
4. D. E. Bartine
5–9. B. L. Bishop
10–14. T. A. Gabriel
15. R. A. Lillie
16. F. C. Maienschein
17. R. W. Peelle
18. RSIC
19. R. T. Santoro
20. A. Zucker
21. P. W. Dickson, Jr. (Consultant)
22. G. H. Golub (Consultant)
23. D. Steiner (Consultant)
24–25. Central Research Library
26. ORNL Y-12 Technical Library Document Reference Section
27–28. Laboratory Records
29. ORNL Patent Office
30. Laboratory Records - RC

EXTERNAL DISTRIBUTION

31. Office of Assistant Manager for Energy Research & Development, DOE-ORO, Oak Ridge, TN 37830

32. Argonne National Laboratory, Library Services Department, 302-CE125, 9700 S. Cass Avenue, Argonne, IL 60439

33. T. W. Armstrong, Science Applications, Inc., PO Box 2807, La Jolla, CA 92038

34. Miguel Awschalom, National Accelerator Laboratory, PO Box 500, Batavia, IL 60510

35. V. S. Barashenkov, Laboratory of Theoretical Physics, Joint Institute for Nuclear Research, Head Post Office, PO Box 79, Moscow, USSR

36. Dr. Gerald W. Bennett, Brookhaven National Laboratory, Upton, NY 11973

37. D. Berley, National Science Foundation, Washington, DC 20550

38. Dr. Elliott Bloom, Stanford Linear Accelerator Center, PO Box 4349, Stanford, CA 94305

39. J. Brau, University of Tennessee, Dept. of Physics, Knoxville, TN 37919

40. Dr. Bruce Brown, Fermi National Accelerator Laboratory, PO Box 500, Batavia, IL 60510

41. Dr. David O. Caldwell, Department of Physics, University of California at Santa Barbara, Santa Barbara, CA 93106

42. Stanley B. Curtis, Lawrence Radiation Laboratory, Bldg. 29, Room 213, Berkeley, CA 94720

43. Herbert Destaebler, Stanford Linear Accelerator Center, Stanford University, Stanford, CA 94305

44. R. D. Edge, Physics Department, University of South Carolina, Columbia, SC 29208

45. Dr. R. Eisenstein, Department of Physics, University of Illinois, Urbana, IL 61801

46. R. W. Ellsworth, George Mason University, Fairfax, VA 22030

47. Dr. Chris Fabjan, CERN, Geneva 23, Switzerland

48. Dr. G. Feldman, Stanford Linear Accelerator Center, Stanford University, Stanford, CA 94305

49. Dr. W. T. Ford, Experiment lA-Lab C, Fermi National Accelerator Laboratory, PO Box 500, Batavia, IL 60510

50. Dr. E. Fowler, Department of Physics, Purdue University, West Lafayette, IN 47907

51. H. T. Freudenreich, University of Maryland, College Park, MD 20742

52. E. Freytag, Deutsches Elektronen-Synchrotron, DESY, 2 Hamburg Dr., Flottbek, Notkesteig l, W. Germany

53. Dr. G. T. Gillies, Department of Physics, University of Virginia, Charlottesville, VA 22901

54. Dr. Gary E. Gladding, University of Illinois, Department of Physics, Urbana, IL 61801

55. K. Goebel, Health Physics Group, CERN, 1211 Geneva 23, Switzerland

56. J. A. Goodman, University of Maryland, College Park, MD 20742

57. Dr. M. Goodman, Department of Physics, Harvard University, Cambridge, MA 02138

58. Dr. Herman Grunder, Deputy Director, General Sciences, Lawrence Berkeley Laboratory, Bldg. 50A, Room 4119, 1 Cyclotron Rd., Berkeley, CA 94720

59. H. J. Hargis, University of Tennessee, Department of Physics, Knoxville, TN 37919

60. Frenc Hajnal, Health and Safety Laboratory, U.S. Department of Energy, 376 Hudson St., NY, NY 10014

61. M. Hofert, CERN, 1211 Geneva 23, Switzerland

62. Mr. Terrence Jensen, Dept. of Physics and Astronomy, The University of Rochester, Rochester, NY 14627

63. Prof. D. Lal, Tata Institute of Fundamental Research, National Centre of the Government of India for Nuclear Science & Mathematics, Homi Bhabha Rd., Bombay 5, India

64. Lawrence Livermore Laboratory, Technical Information Department, PO box 808, Livermore, CA 94550

65. V. Lebedev, Institute of High Energy Physics, Serpukhov, Moscow Region, USSR

66. Library for Nuclear Science, Massachusetts Institute of Technology at Middleton, Middleton, MA 01949

67. Dr. J. LoSecco, Department of Physics, California Institute of Technology, Pasadena, CA 91125

68. Dr. J. Marks, Accelerator Fusion Research Division, Lawrence Berkeley Laboratory, Bldg. 50, Room 149, 1 Cyclotron Rd., Berkeley, CA 94720

69. A. I. Mincer, University of Maryland, College Park, MD 20742

70. Dr. V. S. Narasimham, Tata Institute of Fundamental Research, Bombay 400 005, India

71. W. R. Nelson, Stanford Linear Accelerator Center, Stanford University, PO Box 4349, Stanford, CA 94305

72. Keran O'Brien, Health and Safety Laboratory, U.S. Department of Energy, 376 Hudson St., NY, NY 10014

73. Dr. T. R. Palfrey, Jr., Department of Physics, Purdue University, West Lafayette, IN 47907

74. Dr. Robert Palmer, Brookhaven National Laboratory, Upton, NY 11973

75. Dr. C. W. Peck, Department of Physics, California Institute of Technology, Pasadena, CA 91109

76. J. Ranft, Karl-Marx University, Physics Section, Linnestrasse 5, 701 Leipzig, W. Germany

77. Dr. Lincoln Reed, Division of High Energy and Nuclear Physics, Department of Energy, Washington, DC 20545

78. Dr. C. Rubbia, Lyman Laboratory, Harvard University, Cambridge, MA 02138

79. Dr. W. Schmidt, Institute of Experimental Nuclear Physics, University of Karlsruhe, 75 Karlsruhe, W. Germany

80. The Secretary, Radiation Group, Lab II, CERN, 1211 Geneva 23, Switzerland

81. Dr. Walter Selove, University of Pennsylvania, Department of Physics, Philadelphia, PA 19104

82. B. S. P. Shen, Department of Astronomy, University of Pennsylvania, Philadelphia, PA 19104

83. Dr. M. Shupe, Department of Physics, University of Minnesota, Minneapolis, MN 55455

84. Stanford Linear Accelerator Center, Attention: Library, PO Box 4349, Stanford, CA 94305

85. Dr. Alan Stevens, Physics Department, Brookhaven National Laboratory, Upton, NY 11973

86. G. R. Stevenson, Radiation Protection Group, Lab II, CERN, 1211 Geneva 23, Switzerland

87. Dr. L. Sulak, Department of Physics, University of Michigan, Ann Arbor, MI 48109

88. R. F. Taschek, Los Alamos National Laboratory, P.O. Box 1663, Los Alamos, NM 87544

89. R. Tesch, DESY, Hamburg, Notkesteig 1, W. Germany

90. Ralph H. Thomas, University of California, Lawrence Radiation Laboratory, Health Physics Department, Bldg.72, Berkeley, CA 94720

91. V. D. Toneev, Laboratory of Theoretical Physics, Joint Institute for Nuclear Research, Head Post Office, PO Box 79, Moscow, USSR

92. S. C. Tonwar, University of Maryland, College Park, MD 20742

93. W. Turchinetz, Massachusetts Institute of Technology, R26-411, Cambridge, MA 02139

94. Dr. W. J. Willis, CERN, Geneva 23, Switzerland

95. Dr. D. Winn, Lyman Laboratory, Harvard University, Cambridge, MA 02138

96. Dr. J. Wilcznski, Nuclear Research Center, Karlsruhe, W. Germany

97. Dr. S. Yellin, Stanford University, Stanford Linear Accelerator Center, P.O. Box 4349, Stanford, CA 94305

98. G. B. Yodh, University of Maryland, College Park, MD 20742

99. Dr. B. Zeitnitz, Nuclear Research Center, Karlsruhe, W. Germany

100–126. Technical Information Center, PO Box 62, Oak Ridge,TN 37831